Photodiagnosis and Photodynamic Therapy 28 (2019) 25–37

Contents lists available at ScienceDirect

Photodiagnosis and Photodynamic Therapy

journal homepage: www.elsevier.com/locate/pdpdt

A simple strategy for chemo-photothermal ablation of breast cancer cells by novel smart gold nanoparticles

Zahra Poursalehi[a], Roya Salehi[b,*], Nasser Samadi[c], Seyed Hossein Rasta[d], Behzad Mansoori[e], Hasan Majdi[a]

[a] Department of Medical Nanotechnology, Faculty of Advanced Medical Sciences, Tabriz University of Medical Sciences, Tabriz, Iran
[b] Drug Applied Research Center and Department of Medical Nanotechnology, Faculty of Advanced Medical Sciences, Tabriz University of Medical Sciences, Tabriz, Iran
[c] Department of Biochemistry and Clinical Laboratories, Faculty of Medical Sciences, Tabriz University of Medical Sciences, Tabriz, Iran
[d] Department of Medical Bioengineering, Tabriz University of Medical Sciences, Tabriz, Iran
[e] Immunology Research Center, Tabriz University of Medical Sciences, Tabriz, Iran

ARTICLE INFO

Keywords:
Photothermal effect
Smart gold hydrosol
Doxorubicin
Combination therapy
Apoptosis

ABSTRACT

Combined therapeutics dependent on the synergistic effect between photothermal therapy (PTT) and chemotherapy have been anticipated to be the next generation of cancer treatment.

For this purpose, a novel gold hydrosol was synthesized by a one-pot approach using poly (2-(dimethylamino) ethyl methacrylate-co- N-isopropylacrylamide-co- 2-vinylpyridine) P(DMAEMA-co-NIPAAM-co-VP) terpolymers as a reducing and stabilizing agent. The synthesized gold hydrosol was recoated by a novel carboxylic acid rich poly (N-isopropyl acrylamide-co-maleic anhydride-graft-citric acid) (PNIPAAm-co-PMA-g-CA) copolymer. Then the gold nanoparticles conjugated with Doxorubicin (DOX) and served as a smart photo synthesizer for chemo/photothermal therapy of MCF-7 breast cancer cells. The synthesized nanoparticles had mono-dispersed spherical morphology with a diameter below 30 nm. Our results from cellular uptake indicated that around 100% of the particles were uptake by MCF-7 cells in the first 3 h of exposure time. The temperature of nanocomposites considerably went up to 45 °C with 10 min exposure to near-infrared irradiation.

As a striking result, a single round of PTT combined with a sub-therapeutic dose of DOX revealed a synergistic effect with an ability of robust anti-tumor response up to 99.99% (sum of the population of apoptotic and necrotic cells) demonstrated by Annexin-V, cell cycle and DAPI staining techniques.

In conclusion, Near-infrared-mediated photothermal conversion exhibited high effectiveness of a combinational chemo-thermotherapy to treat cancer cells.

1. Introduction

There is a crucial need to develop novel strategies for cancer therapies to eradicate solid tumors and metastatic nodes, while concurrently inhibiting tumor recurrence.

Chemotherapeutic agents, as a traditional cancer therapy method, destroy the tumor cells, that grow and divide quickly, but the rapidly growing normal cells, for example blood cells, cells of the mucous membrane lining the internal organs, and hair follicles are affected by these drugs [1].

Compared with traditionally used chemotherapy and radiotherapy, thermal destruction of cancerous cells with photothermal therapy (PTT) is a minimally invasive method for eradicating of local tumors [2–4]. Whereas the absorption of hemoglobin, melanin, and water in NIR regain is reduced and the optical window in this regain allowing deeper light penetration into fluids and tissues; NIR lasers are commonly used in plasmonic nanoparticle-induced PTT [5]. Visible light has been applied for surface epithelial cells or in transparent tissues (e.g. the eye), assisting in operating ablation of cells or photo cauterization of blood NIR [6].

The organelles in a cell have been supplied with biological photothermal vehicles (e.g. hemoglobin and cytochromes) with low absorption efficacy [5,7,8]. To improve the photothermal outcome, photosensitizers are used to transport to cancer cells and eradicate malignant cells [7].

Plasmonic metal nanoparticles as nanoparticle-based photosensitizers have the ability to be uptake to the tumor tissue. These particles also can generate local heat up to 42–45 °C when they are

* Corresponding author.
E-mail address: salehiro@tbzmed.ac.ir (R. Salehi).

https://doi.org/10.1016/j.pdpdt.2019.08.019
Received 3 May 2019; Received in revised form 22 July 2019; Accepted 12 August 2019
Available online 24 August 2019
1572-1000/

exposed to the laser [9]. Therefore cancer-specific hyperthermic treatment can be induced by selectively delivering heat to cancer cells which diminishes the damage to non-targeted tissues higher susceptibility to chemotherapy [10]. Gold nanoparticles (AuNPs) used for thermal ablation of tumor cells, are inert photosensitizers that expose strong surface plasmon resonance (SPR) and produce heat by electromagnetic radiation and electron excitation and relaxation [2,11]. NIR-absorption via AuNPs is usually required a rough surface and/or anisotropic morphology [12–16]. However, stabilizing of anisotropic structures of gold nanoparticles such as nanorod, nanocage, nanoshell and hollow nanosphere, NIR-absorption via AuNPs usually needs a rough surface and/or anisotropic morphology [12–16]. Although, stabilizing of anisotropic structures of gold nanoparticles is difficult but they have a suitable range of absorption in NIR, [17–23].

PTT method is limited to local tumors, and utilizing of that in dispersed and metastatic tumors which are far away from the source of NIR, cannot be practical [3]. With regard to this issue, to improve efficacy of this therapeutic method, combined methods have been created. [24–29].

Tumor environment is more acidic nutrient-deficient, and hypoxic than normal tissues, which are supposed to enhance the vulnerability of cancer cells to heat [6,7].

Combined therapy, based on chemotherapy and hyperthermia among other combined therapies have attracted lots of attentions [30]. Since DNA repair procedures are temperature-dependent, DNA damaging agents including Doxorubicin (DOX), are more practical in combination with thermal therapy [30,31]. DOX mainly prevents the topoisomerase I and II and bind into DNA, and causes the planned cell death, which quickly targets dividing cells and late disease expansion [32].Various methods have been proposed for the synthesis of AuNPs [33–35].

Synthesis of gold hydrosols was obtained in a one-step route by reduction of aqueous solutions of metal salts via well-dispersed polymers. In this study, for the first time, very stable gold nanoparticles were synthesized in the presence of poly (2-(dimethylamino) ethyl methacrylate-co- N-isopropylacrylamide-co- 2-vinylpyridine) P (DMAEMA-co-NIPAAM-co-VP) terpolymers as reducing and stabilizing agent. DEAEMA was chosen as a reducing agent and stabilizer, VP is one of the commonly consumed nonionic polymers for stabilizing metal nanoparticles and NIPAM applied as a hydrated layer to increase the stability of gold nanoparticles [36–40]. Polymer chains were chemically absorbed on the nanoparticles thus, they cause colloidal stabilization. Then synthesized polymer-coated AuNPs was recoated by novel super carboxylic acid containing copolymer (by opening anhydride maleic ring with the aid of citric acid and vinyl copolymerization with NIPAAm) in order to have pH-responsive nanoparticle with high DOX interaction at the physiological environment and tumor assistant drug release. Then the combined chemo-photothermal therapy was investigated in MCF-7 breast cancer cell line in the presence of newly engineered nanoparticle.

2. Experimental

2.1. Materials

Hydrogen tetrachloroaurate (III) hydrate (HAuCl4) ≥99.9%, *N*-isopropyl acrylamide (NIPAAm, purity of 99%,), maleic anhydride (MA), dimethylamino ethyl methacrylate (DMAEMA 98%), N-Vinylpyrrolidone (VP) (purified by vacuum distillation) 4′,6-Diamidino-2-Phenylindole, Dihydrochloride (DAPI),3-(4,5-dimethylthiazol-2-yl)-2,5-diphenyltetrazolium bromide (MTT), propidium iodide (PI), ribonuclease A, and rhodamine B were purchased from Sigma- Aldrich Co (Steinheim, Germany). 2, 2′- Azobis (isobutyro nitrile) (AIBN, 98%) and ammonium persulfate (APS) were obtained from Sigma- Aldrich Co (Steinheim, Germany) and recrystallized in ethanol twice before using. Citric acid (99.5%) and solvents such as dimethyl formamide (DMF), tetrahydrofuran (THF) and diethyl ether were purchased from Merck Co. THF was purified using solid sodium. Other materials used in biological protocols, including trypsin, fetal bovine serum (FBS), and Roswell park memorial institute 1640 growth medium (RPMI) were purchased from Gibco brl life technologies. Doxorubicin was obtained from Sobhan Pharmaceuticals Co. (Iran). Phosphate-buffered saline Pharmaceutical Co. (Iran) (PBS).Water was deionized and purified with a resistance of 18 MΩ.

2.2. Synthesis

2.2.1. Synthesis of P(NIPAAm-co-DMAEMA-co-VP) three block copolymer (TBP)

N-isopropyl acrylamide (NIPAAm) was purified by recrystallization in hexane and dried under vacuum at 25 °C. VP was freed from stabilizer by twice vacuum distillation with continuous bubbling argon. Then NIPAAm, (1.695 g, 0.015 mol), VP (1.667 ml, 0.015 mol) and DM AEMA (2.355 ml, 0.015 mol) were added in 10 ml deionized water. The mixture was stirred under nitrogen flow for 10 min and then 0.3 mol % AIBN was added to the reaction mixture as the initiator and the polymerization was continued at room temperature under the nitrogen flow and stirred at 750 rpm overnight. After completing the reaction; unreacted monomers, catalysis and other impurities were removed by a dialysis bag with 2000 Da cutoff.

2.2.2. One-pot in situ synthesis of colloidal gold nanoparticles AuNPs in the amine rich polymeric matrix

In situ reduction of gold (III) chloride trihydrate ($HAuCl_4$) to AuNPs with P(NIPAAm-co-DMAEMA-co-VP) three block copolymer (TBP) as reducer and stabilizer agents was done by one-pot synthesis at mild conditions (room temperature and neutral pH). At first, 0.01 g of TBP was dissolved in deionized water and added to 50 μL of 10 Mm at room temperature and stirried at 750 rpm for overnight. Colloidal AuNPs is gradually synthesized by TBP as a reducing and stabilizing agent. Eventually, a wine red solution has been appeared; as time passed, the intensity of red color has been increased. The synthesized TBP decorated-gold nanoparticles (TBP@AuNPs) were filtered using an amicon filter with 100,000 Da cutoff, centrifuged and analyzed using UV–vis spectra (Cecil UV, UK). The molar concentration of synthesized AuNPs was determined by atomic absorption spectroscopy (AAS).

2.2.3. Synthesis of P(NIPAAm-MA-g-CA) super acid polymer (SAP)

Part 1: N-isopropyl acrylamide (NIPAAm: 0.565gr, 0.005 mol) and maleic anhydride (MA: 0.735 g, 0.0075 mol) as monomers were dissolved in 80 mL tetrahydrofuran (THF), and the solution was exposed to the argon flow for 30 min. Then, AIBN (0.3 mol % of all the monomers) was added to the solution as initiator and the reaction flask was heated to 75 °C under an argon atmosphere with continuous mechanical stirring for 24 h. The NIPAAm-co–MA copolymer was gathered from the reaction mixture by precipitation with diethyl ether and dried under vacuum.

Part 2: The product of "part 1" was dissolved in 10 mL DMF and added dropwise to the citric acid (CA: 1.55gr, 0.0081 mol) that dissolved in 5 ml DMF then 50 μL triethylamine was added as a catalyzer. The mixture was purged with the nitrogen gas for 30 min and heated to 75 °C under nitrogen atmosphere with continuous mechanical stirring for 24 h. The copolymer that is full of the acid groups (four carboxylic acid group in each monomer unit) with reddish orange color was produced and separated from the reaction mixture by precipitation with diethyl ether and dried freeze dryer.

2.2.4. Decoration of TBP@AuNPs with SAP

400 μL of SAP solution (0.2 g/mL) in deionized water; was added in 1 mL TBP-AuNPs and stirred at 750 rpm for overnight. The sample was centrifuged with 10KDa Amicon filter at 5000 rpm for 10 min. Composite- like SAP@TBP@AuNPs was obtained.

2.3. DOX loading in SAP@TBP@AuNPs

DOX loading on SAP@TBP@AuNPs was done as follow: Firstly, 525 μL DOX.HCl solutions at the concentration of 2000 μg/mL was dissolved in 3 mL SAP@TBP@AuNPs aqueous solution containing 236 μg/mL of Au nanoparticle and 0.24 g of polymer and the mixture was stirred overnight at room temperature under the dark situation. Thereafter, the solution was centrifuged with 10KDa Amicon filter at 5000 rpm for 10 min to remove the unloaded DOX.HCl. The quantity of DOX in the gathered supernatant was assessed by measuring absorbance at 488 nm. By using UV–vis spectroscopy, and DOX calibration curve, the amount of unloaded DOX were measured. Drug encapsulation efficiency (DEE) and drug loading efficiency (DLE) are calculated by two following formulas:

$$\mathrm{DEE}(\%) = \frac{\text{Mass of drug in nanocarrier}}{\text{Mass of feed drug}} \times 100$$

$$\mathrm{DLE}(\%) = \frac{\text{Mass of drug in nanocarrier}}{\text{Mass of nanocarrier}} \times 100$$

2.4. Characterization of the prepared NC

To analyze the particles size and morphology, transmission electron microscopy (TEM) (LEO 906, Germany) and field effective scanning electron microscopy (FESEM-EDX; S4160 Hitachi, Japan) were employed. We prepared around 100 μL of nanoparticles suspension in aqueous solution at room temperature. The solution was transferred onto a carbon film coated on a copper grid of TEM subsequently freeze drying and observed at 80KV. The powder sample was spread on a SEM stub and sputtered with gold. Particle size was obtained by measuring the diameters of at least 300 particles shown in SEM using image analysis software (Image-Pro plus 4.5; Media Cybernetics, Silver Spring, USA). Zeta-potential and hydrodynamic size measurements were carried out by using (Zetasizer Nano ZS90; Malvern Instruments, Malvern, UK). A double beam UV–Vis spectrophotometer (UV-160, Shimadzu Corporation, Kyoto, Japan) was employed for absorbance measuring by 700 μL quartz cuvette with 10 mm path length.

The chemical composition of the synthesized polymers was determined by Hydrogen nuclear magnetic resonance (^{1}H NMR) spectroscopy using Bruker spectra spin 400 MHz (Germany) and Fourier transforms infrared (FTIR) spectroscopy from Bruker Tensor 27 spectrometer, Germany was utilized for KBr pellet method performing.

2.5. Cell culture

MCF-7 breast cancer cell line and human umbilical vein endothelial cells (HUVECs) were purchased from Pasteur Cell Bank (Tehran, Iran). The selected cell lines were grown in complete medium containing RPMI1640 (Thermo-scientific), and Gibco DMEM/ F12 10% containing Fetal bovine serum (FBS), and 1% Penstrep (Thermo-scientific) in thermal and atmospheric conditions of 37°C, 5% CO2, and 95% humidity.

2.6. Cellular uptake studies

Flow cytometric analysis was carried out to determine the cellular uptake of nanoparticles against the MCF-7 cell line. Rhodamine-B was labelled to SAP@TBP@AuNPs and DOX-loaded SAP@TBP@AuNPs. To prepare rhodamine-B labelled NPs, an aqueous solution of rhodamine-B and NPs (with the ratio of 1/100) was prepared and stirred overnight at room temperature under dark condition. Afterwards the rhodamine-B labelled NPs were separated from free rhodamine-B by dialysis for 24 h using dialysis membrane (Cellu SepH1) with MWCO of 2000 and the external aqueous solution was removed repeatedly and displaced with fresh distilled water. For cell uptake studies, MCF7 cells at the density of 250,000 per well were seeded in 6 well plates and incubated for 24 h. Then the cells were treated with a defined concentration of rhodamine-B labelled NPs (with and without DOX). The cells with no treatment were used as negative control. Respectively After 0.5 h, 1.5 h, 3 h residual NPs was removed and washed with PBS. Then the cells were trypsinized, washed with PBS and examined with FACScalibur flow-cytometer (Becton Dickinson Immunocytometry Systems, San Jose, CA, USA) to measure the fluorescent intensity associated with rhodamine-B uptake inside the cells. The intracellular uptake of NPs was further confirmed by fluorescence microscopy. The cells were grown on coverslips in a 6-well culture plate. After 24 h the cells were treated with rhodamine-B labelled NPs (with and without DOX). After incubation for 0.5, 1.5 and 3 h, the cells were washed with PBS. The coverslips were fixed onto the glass microscope slides, and rhodamine-B labelled nanocarrier uptakes were observed using a fluorescence microscope (Olympus microscope Bh2- FCA, Japan).

2.7. Cell viability assay

The relative cytotoxicity of nanocarrier and the antitumor activity of the free DOX and DOX-loaded SAP@TBP@AuNPs were assessed on the MCF7 cells using the MTT assay method. MCF7 cells were seeded with a density of 10,000 cells per well on 96-well culture plates. After 24 h, the cells were treated with different concentrations of blank SAP@TBP@AuNPs, DOX-loaded SAP@TBP@AuNPs and free DOX and further incubated for 72 h. Then, the cells were washed with PBS gently. Fifty microliters of MTT stock solution (MTT powder was dissolved in PBS at a concentration of 5 mg/mL) and the 150 μL medium were added to detect the metabolically active cells, and the cells were incubated for 4 h until a purple color developed. The media were discarded, and 200 μL of DMSO was added to each well to solubilize water-insoluble formazan salt. Then, the optical densities of each well in the plates were measured by an ELISA plate reader (Awareness Technology, Palm City, FL, USA) at 570 nm. Mean and standard deviation of triplicates was calculated and plotted.

2.8. Cell viability assay after photothermal treatment

MCF7 cells were seeded in 12 well plates at 250 000 cells per well and cultured overnight. The medium was removed and treated with samples (DOX-loaded SAP@TBP@AuNPs and free DOX at IC50 concentration of DOX and blank SAP@TBP@AuNPs) and incubated overnight. The cells were exposed to laser irradiation (810 nm, 0.5 W/cm^2, 10 min) and incubated for 24 h at 37 °C. The cells were exposed to laser irradiation (810 nm, 0.5 W/cm^2, 10 min) set as controls and washed with PBS (pH 7.4). Cell viability after laser irradiation was assessed using an MTT assay method mentioned above.

2.9. Investigation of the combined chemo-photothermal therapy effect

2.9.1. DAPI staining studies

DAPI staining was done for visualization of the condensed and fragmented nuclei of apoptotic cells by NPs (NC, free DOX, and DOX-NC). Briefly, MCF7 cells were seeded on glass coverslips (6 mm) in 12-well plates (250,000 cells per well) and incubated for 24 h. Then the attached cells were treated with DOX-loaded NC and free DOX at the IC50 values of DOX (7.3 μg.mL^{-1}), as well as blank nanocarrier (5 ppm). After 48 h, the cells were exposed to laser irradiation and incubated for 24 h. The cells were exposed to laser irradiation (810 nm, 0.5 W/cm^2, 10 min) set as controls. Then the cells were washed with PBS (Sigma) and fixed by 10% formaldehyde (Merck), then cells were permeabilized by Triton X-100 (Sigma) for 15 min. After proper washings, the cells were stained with DAPI (Sigma) for 5 min. Finally, the apoptotic nuclei (fragmented or wrinkled) were visualized by a Fluorescence microscope (Olympus).

2.9.2. Flowcytometric annexin-v/ pi apoptosis assay

Cells were seeded in 12-well plates with a density of 250,000 cells per well and incubated for 24 h to be attached. Then the attached cells were treated with DOX-loaded NC and free DOX at the IC50 values of DOX (7.3 μg.mL^{-1}), blank nanocarrier (5 ppm) and also non-treated cells. Then the cells were exposed to laser irradiation (810 nm, 0.5 W/cm^2, 10 min) set as controls. After 72 h post final incubation and 24 h after irradiation, the cells were trypsinized, collected and centrifuged to remove the supernatant. Afterward the collected cells were washed one more time with cold PBS to remove all trypsin. Cells were suspended in 200 μL annexin binding buffer. To stain the apoptotic cell, a FITC/annexin-V apoptosis detection kit was applied according to the manufacturer's protocol using 100 μL cell suspensions, 5 μL FITC/annexin-V and 5 μL PI (propidium iodide, provided in the kit). The cells were incubated for 15 min in the dark at room temperature, and then 400 μL of binding buffer was added to each suspension finally, a FACs Calibur flow cytometer was used to analyze the Apoptotic cells (Becton Dickinson).

2.9.3. Cell cycle study

MCF7 cells were seeded with starting populations of 5×10^5 and allowed to reach 80% confluence. After 24 h, the cells were treated with DOX-loaded NC and free DOX at the IC50 values of DOX (7.3 μg.mL^{-1}), blank nanocarrier (5 ppm) and also non-treated cells and cells were exposed to laser irradiation (810 nm, 0.5 W/cm^2, 10 min) set as negative and positive controls. The effects of treatments on cellular cycle were assessed after 72 hof treatment (after treatment the cells were incubated for 48 h and then exposed to laser irradiation followed by 24 h incubation after irradiation. Then, the cells were harvested by trypsinization fand proper PBS washings. Then the cells were fixed in cold ethanol. After 3 days incubation at 4 °C, cells were washed and treated with Ribonuclease A (Cinaclone), with subsequent addition of propidium iodide (PI) (Sigma) at dark. The fluorescence signals were detected by FACS set from Beckton Dickinson Company.

2.10. Statistics of the study

The experiments for each step have been performed in three repeats and the results were reported as mean ± SD. The ANOVA one way or two way was used for comparison of significance among groups. The differences were reflected significances where probability value was calculated < 0.05 by SPSS software.

3. Results and discussion

3.1. Characterization

3.1.1. Characterization of the poly (NIPAAm-co-DMEAMA-co-VP) and poly (NIPAAm-co-MA-CA) copolymers

The chemical composition of the copolymers was determined with ^{1}HNMR, ^{13}CNMR and FTIR by integrating the signals pertaining to each monomer. As an example, Fig. 1a shows ^{1}H NMR spectra of poly (NIPAAm-co-DMEAMA-co-VP) terpolymer. The signals pertaining to PNIPAAm are found in δ (ppm) = 1,60 (CH_2-CH), δ(ppm) = 1.11(($\underline{C}H_3)_2$CH), δ(ppm) = 3.97(N-$\underline{C}$H-$(CH_3)_2$), δ(ppm) = 2.22(CH-C = O). And the signals pertaining to VP are found in, δ (ppm) = 1.60($\underline{C}H_2$-CH-N),δ(ppm) = 3.1(N-$\underline{C}H_2$-CH2),δ (ppm) = 2.02 (CH_2-$\underline{C}H_2$-CH_2),δ(ppm) = 2.22($\underline{C}H_2$-C = O). The signals appeared in δ (ppm) = 4.4(2H, $\underline{C}H_2$–O-C = O), 3.7 (2H, N-$\underline{C}H_2$–CH_2–O-C = O) and 2.6 (6H ($\underline{C}H_3)_2$–N) pertained to protons of DMAEMA moiety. Fig. 1b shows ^{1}H NMR spectra of poly (NIPAAm-co-MA-g-CA) copolymer. The signals pertaining to PNIPAAm are found in δ (ppm) = 1,1-1.2 (CH2-CH),

δ (ppm) = 1.0(($\underline{C}$H3)2CH), δ (ppm) = 3.97(N-$\underline{C}$H-(CH3)2), δ (ppm) = 2.3-2.4($\underline{C}$H-C = O). And the signals pertaining to MA appeared at 3.0–3.1 and 4.2–4.3 ppm and the signal related to CA appeared at 2.5 ppm. In ^{13}CNMR spectra of poly (NIPAAm-co-MA-CA) the peaks at 162, 171 and 174 ppm were related to the carbon of amide, ester and carboxylic acid of PNIPAAm, PMA and CA respectively (Fig. 1c).

In FTIR spectra of P (NIPAAm-co-DMAEMA-co-VP) three block terpolymer an intense peak at 3431 cm^{-1} can be attributed to the NH group of NIPAAm. The C–H stretching vibration of the polymer backbone is manifested through a strong peak at 2928 cm^{-1}. The peak at 1648 cm^{-1} is corresponded to amide C═O stretching from all three monomer units. The peak at 1740 cm^{-1} was attributed to the ester carbonyl group of DMAEMA. The peak at 1558 cm^{-1} was attributed to the bending vibration of N—H of amide groups (Fig. 2a).

In FTIR spectra of P (NIPAAm-co-MA-g-CA) copolymer, an intense peak at 3486 cm^{-1} was related to the OH of carboxylic acid groups and NH of amide groups. The peak at 2800–2900 cm^{-1} is attributed to the C—H stretching vibration of the polymer backbone. A peak at 1670 cm^{-1} is corresponded to amide C═O stretching of PNIPAAm block and the peak at 1713 cm^{-1} was attributed to the C═O stretching of citric acid and MA. The peak at 1594 cm^{-1} was attributed to the bending vibration of N—H of amide groups (Fig. 2b).

3.1.2. Characterization of polymer coated colloidal gold nanoparticles

In this study, highly stable gold nanoparticle was grown gradually over the course of 24 h in the presence of P (NIPAAm-co-DMAEMA-co-VP) terpolymer matrix as reducing and stabilizing agent at room temperature (Fig. 3). The prepared colloidal three-block polymer-coated gold nanoparticle (TBP@AuNPs) was recoated by the second polymer poly (N-isopropyl acrylamide-co-maleic anhydride-graft-citric acid) (PNIPAAm-co-PMA-g-CA) as a super carboxylic acid polymer (SAP). This second copolymer has four carboxylic acid groups in each unit of maleic anhydride-graft-citric acid (MA-g-CA) monomer (polymer pka was 5.5).

The recorded TEM images display the one-pot synthesis of gold nanoparticles (AuNPs) mediated poly (NIPAAm-co-DMEAMA-co-VP) (TBP@AuNPs) led to successful creation of a large number of homogeneous spherical gold nanoparticles with particles size in the range of 8–13 nm (Fig. 4a). In the second step prepared TBP@AuNPs was recoated with poly (NIPAAm-co-MA-g-AC) (SAP). SAP@TBP@AuNPs was obtained with uniform spherical and core-shell morphology with mean diameter of around 30 nm (Fig. 4b). Furthermore, the use of high-resolution TEM (HR-TEM) obviously reveals the crystalline nature of the nanoparticles along with that they are enclosed by a protected polymer layer (Fig. 4b). Moreover, monodispersity, spherical morphology and size (30 nm) obtained with TEM image is comparable with the results from SEM image (Fig. 4c).

Since these nanoparticles were very small, they have picked up easily by the cells in the high population and acted more effectively in the heat transfer to the different location of a cell [41,42].

In the UV–vis spectra of TBP@AuNPs after coating with SAP and DOX loading, an obvious increase in the NIR region absorption (from OD: 0.05 to 0.2) were observed (Fig. 5a). Fig. 5b shows the stability graph of the SAP@TBP@AuNPs by surface plasmon resonance (SPR). During a long –term storage for 6 months, it was found that there was a very slight blue shift in SPR spectra of these nanoparticles indicating its excellent stability in solution. The total changes at the UV–vis spectra have been in the range of 519 nm–526 nm. This study was performed while the GNP was kept in a soluble state at 4 °C. Fig. 5c, shows the zeta potential of TBP@AuNPs, SAP@TBP@AuNPs and DOX-loaded SAP@TBP@AuNPs. The zeta potential of TBP@AuNPs was positive (+5 mV), while after coating with P(NIPAAm-co-MA-g-AC) (SAP) copolymer the nanoparticles surface charge was decreased to a negative charge (−38 mV) due to the presence of carboxylic acid groups. After DOX loading due to the interaction of positive amine groups of DOX with carboxylic acid groups of the surface coated polymer, the surface charge of NPs was increased to around -20 mV. This surface charge change trend showed the successful decoration of TBP@AuNPs with SAP and DOX. The concentration of gold atoms is 236 μg/mL obtained

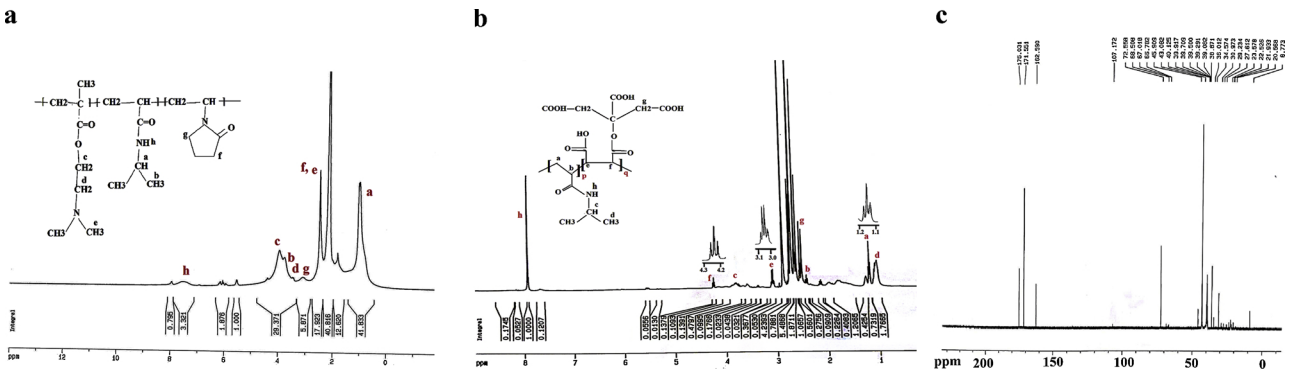

Fig. 1. a)^{1}H NMR spectra of poly (NIPAAm-co-DMEAMA-co-VP) terpolymer.
b)^{1}H NMR spectra of poly(NIPAAm-co-MA-g-CA) copolymer and c)^{13}CNMR spectra of poly(NIPAAm-co-MA-g-CA) copolymer

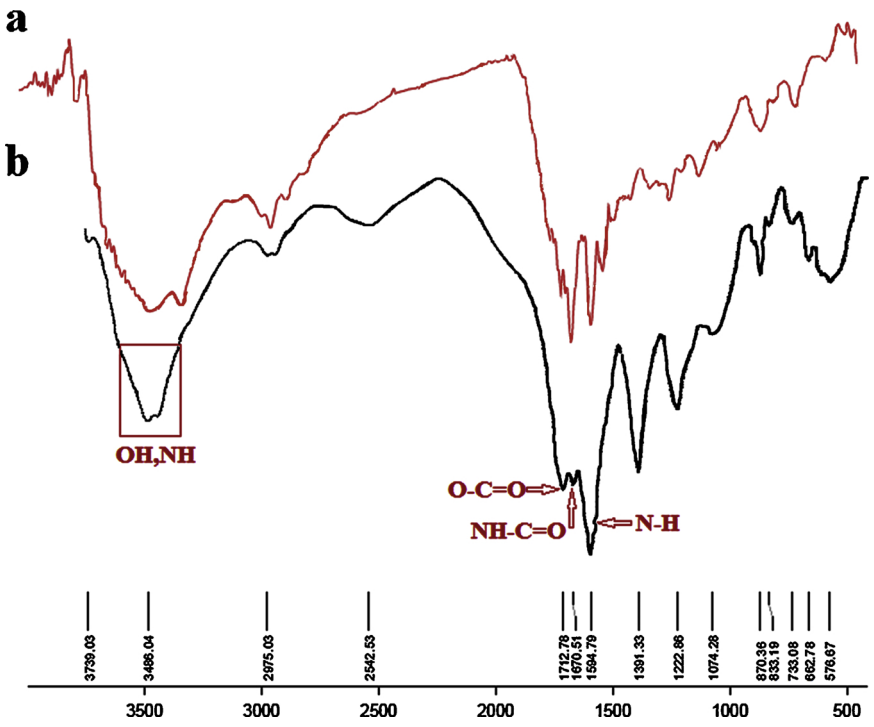

Fig. 2. FTIR spectroscopy of poly (NIPAAm-co-DMEAMA-co-VP) terpolymer and poly (NIPAAm-co-MA-g-CA) copolymer.

by atomic absorption spectroscopy.

Zeta potential is a significant physicochemical parameter that affects the stability of nano-suspensions. The high positive or negative charge of nanoparticles led to larger repulsive forces. On the other hand, the high charge of the particles, whether positive or negative, causes the NPs to be absorbed by the phagocytes of the liver and disposed of the body. In the case of a combined electrostatic and steric stabilization, a zeta potential of ± 20 mV is appropriate [43–48].

3.2. Effect of pH on DOX interaction with SAP@TBP@AuNPs

DOX loading on SAP@TBP@AuNPs was investigated at three different pHs to demonstrate that pH sensitivity of polymer affect the loading process. Under physiological condition (pH 7.4), DOX has a positive charge (pka = 8.3). Furthermore, at these situations, the carboxylic acid functional groups of the SAP@TBP@AuNPs (pka = 5.5) are deprotonated which means they are negatively charged. At pH 7.4, the presence of ionic interaction among the amino ($N-H3^{+}$) functional group in the positively charged DOX molecules and the anionic

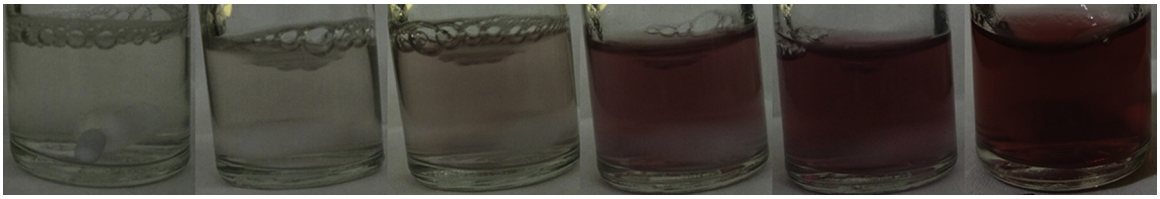

Fig. 3. Gold nanoparticles synthesis by gradual reduction of $HAucl_4$ with P(NIPAAm-co-DMAEMA-co-VP) terpolymer as reducing and stabilizing agent during 24 h at room temperature and natural pH.

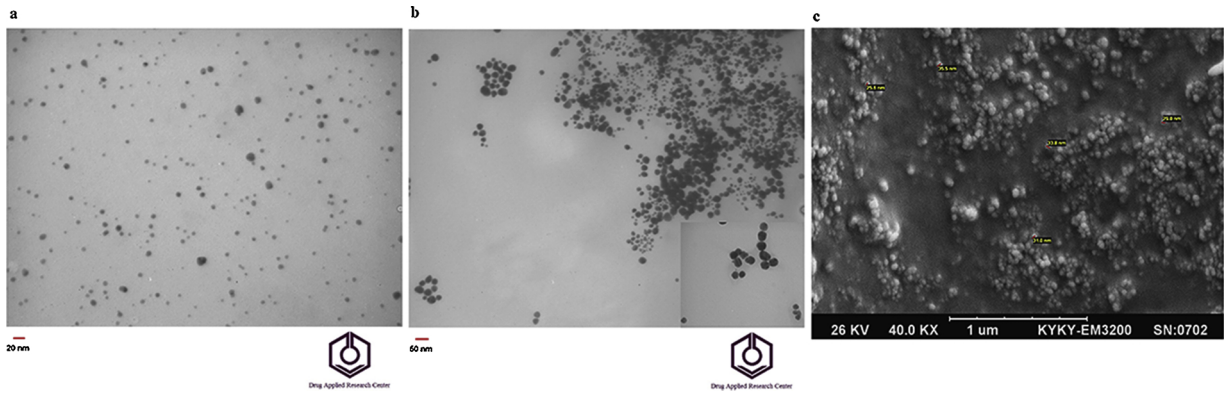

Fig. 4. TEM image of a) poly (NIPAAm-co-DMEAMA-co-VP) coated gold nanoparticles (TBP@AuNPs), b) TEM image of poly (NIPAAm-co-MA-g-CA) coated TBP@AuNPs(SAP@TBP@AuNPs) and c) SEM image of SAP@TBP@AuNPs.

carboxylic acid functional groups (COO) in the SAP@TBP@AuNPs lead to for almost 99.07% of DOX encapsulation efficiency and 19.81% of its loading efficiency (Fig. 6a). UV–vis absorption spectra revealed that DOX loading at PH 14 lead to nanoparticle blue shift and its aggregation (Fig. 6b). At pH below 6, due to the protonation of polymer chain carboxylic group there is not ionic interaction between DOX and SAP@TBP@AuNPs and DOX encapsulation efficiency drop to less than 50% (Fig. 6c).

3.3. Nanocarrier reaction with NIR irradiation

Previous studies revealed that the lasers with wavelengths of 500–550 nm have high absorption in the cell environment so the penetration depth of these wavelengths is very small. Therefore the major number of the cells has not received these photons of energy. On the other hand, the lasers with wavelengths of 800–830 nm (NIR) had low absorbance and high penetration depth in cell environments compared to green wavelength lasers (500–550 nm).

In some studies spherical gold nanoparticles with maximum absorption in the visible region have shown photothermal effects using NIR irradiation [49,50]. On the other hand, in previous studies smart spherical gold nanoparticles that were affected by various stimuli and aggregated, that led to change their absorbing properties from the visible to NIR regain. This property can be inspired to create one approach to increase the capacity of these plasmon nanoparticles in laser therapy [51–53].

The surface plasmon spectra of novel developed NPs in this study showed the slight redshift in the UV–vis spectra of the TBP@AuNPs after coating with SAP and DOX loading were observed (Fig. 5a). The absorption intensity at maximum absorption area of 530 nm (OD: 0.4) which was two-fold larger than the absorption at 803 nm (OD: 0.2). Therefore the difference of received photons energy with NIR laser has been half in comparison with green photons. Because of good penetration depth at NIR region 810 nm laser was chosen for photothermal study. By increasing the exposure time (10 min), every particle inside the cells have received enough energy to react thermally [49,50,54].

Irradiation could also influence the efficiency of the photothermal effect [9,55,56,52,57].

The photothermal induced cells destruction forms altered by temperature variation in PTT. The prior studies demonstrated that the cell killing is ineffectual at low temperatures. While the temperature augmented to 49 °C, the cell death form converted to necrosis dominant. The modest temperature of 46 °C makes necroptosis cell death. Temperature-dependent necroptosis is the main mechanism of inducing cell death in PTT besides apoptosis and necrosis [58].

The temperature change of an aqueous solution of the SAP@TBP@AuNPs and DOX-loaded SAP@TBP@AuNPs (10 ppm) during laser irradiation using an 810 nm NIR laser was studied. The results indicated that after exposure of NPs solution to laser irradiation for 10 min, the temperature was increased from 37 to 45 °C while the temperature of PBS control solution only increased 1.6 °C (Fig. 7).

3.4. Cell uptake

The amount of nanoparticles entering the cell is one of the basic principles for photothermal effect and drug carrier performance because the intracellular photothermal agents can improve the efficiency of photothermal cancer therapy [56]. To form a photothermal phenomenon, the presence of enough nanoparticles in the cells is necessary. Since the amount of nanoparticle entering the cell can have a direct impact on the effectiveness of the therapeutic strategy, high cellular uptake is an advantage. NPs labelled with rhodamine b were used to evaluate the percentage of intracellular absorption of novel developed NPs. *in vitro* cellular uptake of SAP@TBP@AuNPs and DOX-loaded SAP@TBP@AuNPs test were performed using MCF7 (Fig. 8A)

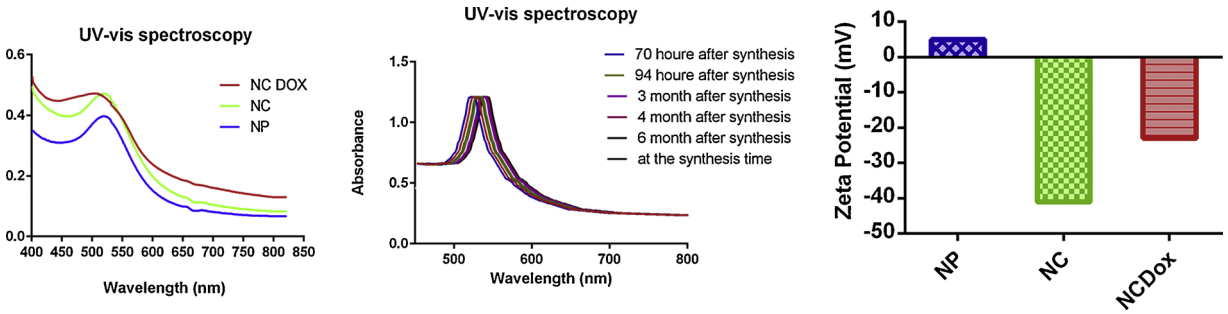

Fig. 5. a) Surface plasmon resonance spectra of TBP@AuNPs (NP), SAP@TBP@AuNPs (NC) and DOX@ SAP@TBP@AuNPs (NC DOX). b) The stability graph of the SAP@TBP@AuNPs (NC) by surface plasmon resonance (SPR) from synthesis until a long –term storage of 6 months, c) the zeta potentional of TBP@AuNPs (NP), SAP@TBP@AuNPs (NC) and DOX-loaded SAP@TBP@AuNPs (NC DOX).

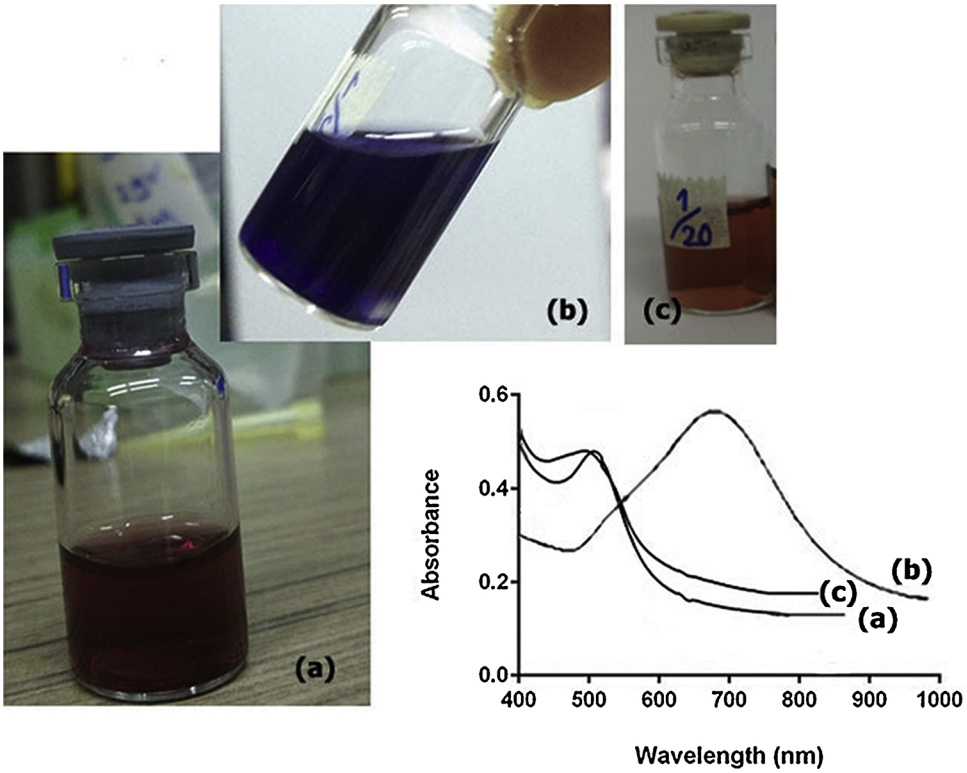

Fig. 6. The effect of pH on DOX loading at SAP@TBP@AuNPs at three pH values a) pH 7.4, b) pH 14 and c) pH 6.

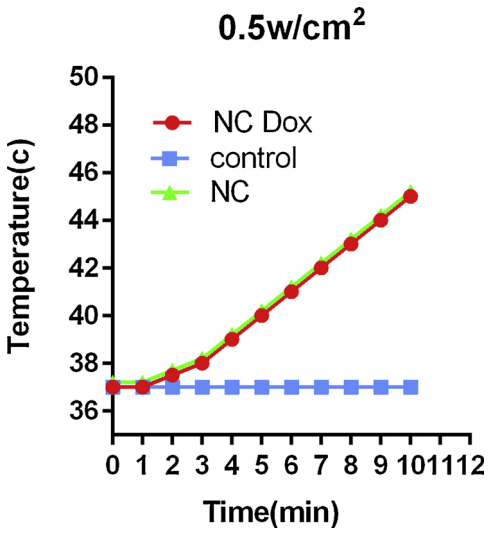

Fig. 7. The temperature change of an aqueous solution of the SAP@TBP@AuNPs (NC) and DOX-loaded SAP@TBP@AuNPs (NC DOX) (10 ppm) at different exposure time during NIR laser irradiation using an 810 nm.

and HUVECs as cancer and normal cell lines (Fig. 8B), respectively. Untreated cells were considered as a control group. Interestingly, fluorescent microscopy image revealed that the internalization of SAP@TBP@AuNPs into the MCF7 cancer cells was obviously higher than the HUVECs normal cells. These results indicated the proper function of the SAP@TBP@AuNPs in targeting of cancer cells. More accurately quantification of the SAP@TBP@AuNPs and DOX-loaded SAP@TBP@AuNPs uptake efficiency in MCF7 cell line was studied by flow cytometry. Fig. 8b showed the percentage of NPs uptake by cells. The results indicated that SAP@TBP@AuNPs uptake to MCF-7 cells was increased in a time-dependent manner and reached from 64% at 0.5 h exposure time to 99% after 3 h. Also, DOX-loaded SAP@TBP@AuNPs uptake reached around 100% at first 0.5 h of exposure. The result of intracellular absorption of NPs studied with fluorescence microscope has confirmed the results of the flow cytometry technique.

3.5. Cytotoxicity assay

Cell viability assay is required once generating a novel drug delivery system to avoid nonselective cytotoxic events. Particle-made cytotoxicity was quantified with the MTT assay, a tactic widely used to estimate the mitochondria activity to measure the cell growth or cell death [34,45]. The toxicity of the SAP@TBP@AuNPs was investigated by an MTT assay. Fig. 9a showed cell viabilities of MCF7 breast cancer cells treated with different concentrations of gold nanoparticles (1.25–20 μg/mL) decorated with TBP@AuNPs and SAP@TBP@AuNPs after incubation for 48 h. The gold nanoparticle concentration in TBP@AuNPs and SAP@TBP@AuNPs was obtained by atomic absorption spectroscopy. The cells treated with TBP@AuNPs revealed significant cytotoxicity at the concentrations from 5 to 20 μg/mL, with a half maximal inhibitory concentration (IC50) of 8.3 μg/mL showed that they were highly toxic but when the AuNPs was decorated by SAP@TBP@AuNPs, the IC50 change to 31.46 μg/mL. The cytotoxicity was decreased after coating with SAP, somehow the MCF-7 cell viability after treatment with 20 μg/mL of TBP@AuNPs and SAP@TBP@AuNPs increased from 12.5% reach to 74.7% after 48 h incubation. As a result surface coating with SAP not only decreased the toxicity of nanocomposite but also because of the presence of high amount of carboxylic acid groups on the polymer surface, provided an excellent site for pH-responsive ionic interaction with DOX.

Next, the mortality rate of MCF-7 cells treated with DOX-loaded SAP@TBP@AuNPs and free DOX was quantitatively evaluated by MTT assay (concentration of gold nanoparticle was 1.25, 2.5 and 5 ppm) loaded with DOX (concentration of DOX 1.825, 3.6 and 7.3 ppm) (Table 1). We typically used the SAP@TBP@AuNPs at concentration that more than 90% of cells were viable. NCs showed high colloidal

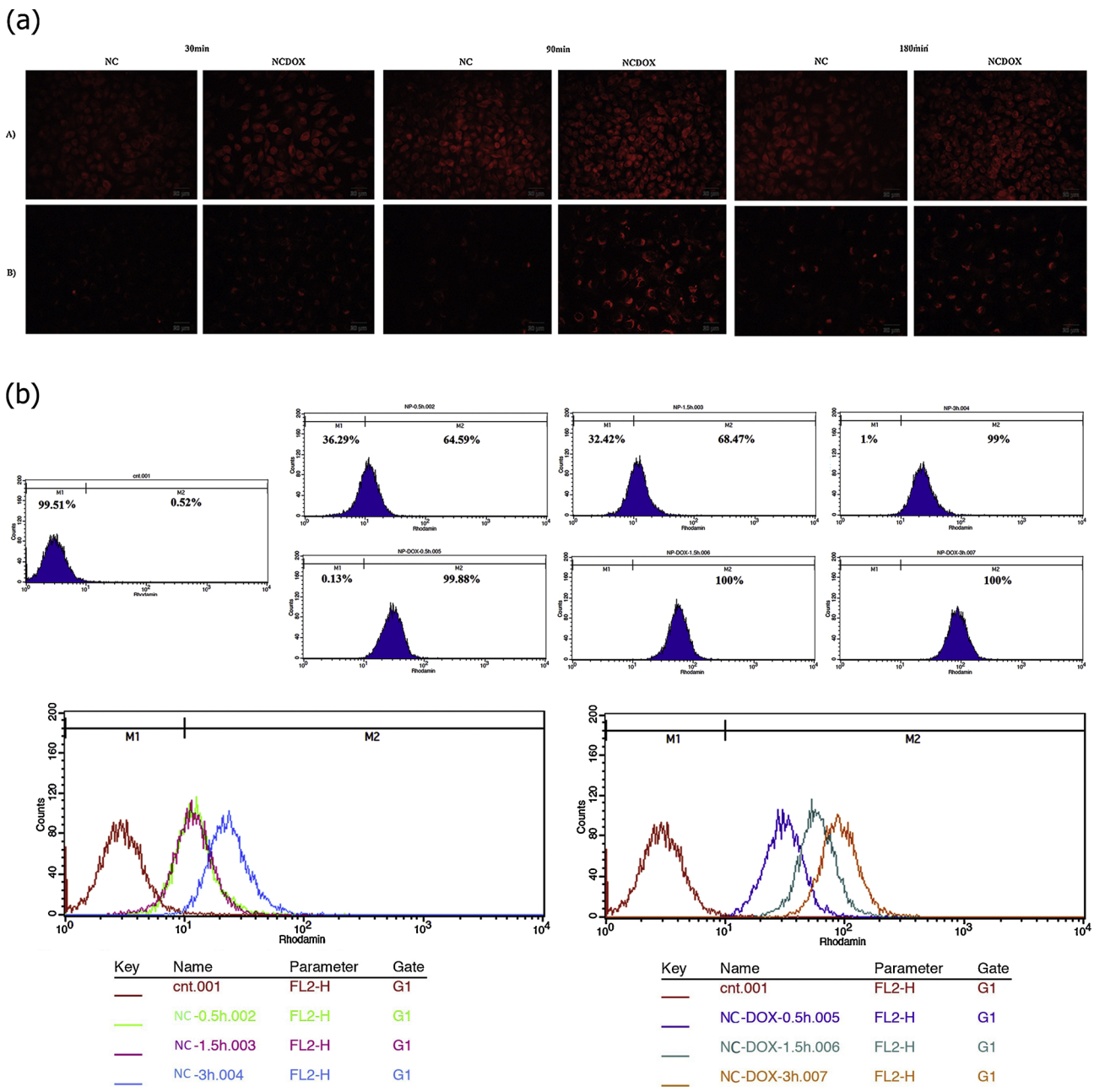

Fig. 8. a) Qualitative cell uptake of MCF7 (A) or Huvec (B) cells lines treated with Rhodamine B-labelled SAP@TBP@AuNPs (NC) or rhodamine B-labelled DOX-loaded SAP@TBP@AuNPs (NCD) for exposure durations of 30, 90 and 180 min captured by florescent microscopy and b) Quantitative results of cell uptake assay obtained by flow cytometry.

stability in serum-containing cell culture media. Cell viability results showed that when cells treated with DOX-loaded SAP@TBP@AuNPs was reduced more than free DOX treatments (Table 1). DOX free NC treatment induced no significant cytotoxicity. More inhibition of MCF-7 cells growth treated with DOX-loaded SAP@TBP@AuNPs compared to free DOX would have advantageous in lowering the dose of the anticancer drug in the application.

3.6. Combined therapy and apoptosis assays

Cell killing efficiency of the antitumor drug, depending on DNA damage, showed the efficiency of therapeutics increased by hyperthermia. DOX as one of the most extensively used anticancer drugs, mainly against breast cancer. Therefore, for the purpose of increasing DOX efficacy against cancer cells, we used combined chemo-photothermal therapy with DOX and AuNPs as heat-generator following irradiation with light.

In order to indicate the improved therapeutic index of chemo-photothermal combination therapy, apoptotic assays including Annexin V-FITC, DAPI staining and cell cycle tests were performed on the cells exposed to DOX nanoformulation with and without NIR irradiation, free DOX, and NIR irradiation alone.

3.6.1. Induction of apoptosis studied by DAPI staining method

The degree of nuclear condensation and fragmentation, as the indications of apoptotic cells, were analyzed using DAPI nuclear staining. To further assess the photothermal effect in the induction of apoptosis, SAP@TBP@AuNPs and DOX-loaded SAP@TBP@AuNPs exposed to NIR irradiation. Then the healthy, apoptotic, and necrotic cells were assessed by determination of the chromatin morphologies with DAPI

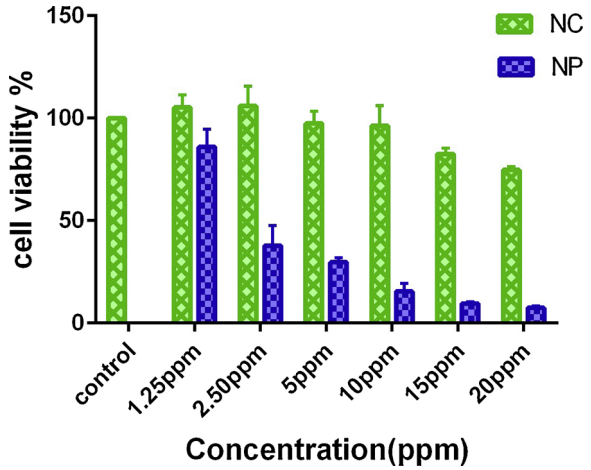

Fig. 9. Cell growth inhibition rates by different concentration of TBP@AuNPs (NP) and SAP@TBP@AuNPs (NC) after 24 h treatment.

Table 1
Mcf-7 cells viability treated with different concentration of free DOX and DOX-loaded NC.

Concentration	Cell viability	
	Free DOX	DOX-loaded NC
1.825	44.48 ± 3.2	39.29 ± 1.2
3.6	16.08 ± 4.5	12.02 ± 3.8
7.3	13.29 ± 1.6	8.21 ± 2.3

staining method. NPs mediated photothermal ablation capably destroyed cancer cells in vitro. MCF7 cells showed relatively low toxicity when incubated with SAP@TBP@AuNPs concentration up to 20 μg/mL. Most of the cells treated with either SAP@TBP@AuNPs alone or NIR irradiation alone (810 nm, 0.5 W/cm^2, 10 min) (Fig. 10). On the other hand, cells treated with DOX alone and DOX-loaded SAP@TBP@AuNPs without laser irradiation showed some changes in their chromatin morphology and apoptosis. But when the cells were treated with SAP@TBP@AuNPs with laser irradiation, a clear increase in nuclear condensation was observed and the cell viability was significantly decreased while neither the SAP@TBP@AuNPs nor the NIR irradiation alone destroyed cells. These results indicated that the AuNPs are necessary as photothermal agents for photothermal conversion of the NIR irradiation. Moreover, the photothermal effect of the DOX-loaded SAP@TBP@AuNPs with laser irradiation led to a large number of dead cells and the considerable number of cells were apoptotic with high chromatin fragmentation (Fig. 10). In this treatment group, nearly all the cells exhibited clear signs of condensed nuclei and massive cell death can be detected. These consequences showed that combination of NPs and NIR irradiation is essential to get a lethal influence on tumor cells. Also, the combination of chemotherapy drug (DOX) loaded in NPs with laser irradiation showed the highest cancer therapy efficacy. DOX-loaded SAP@TBP@AuNPs with laser irradiation resulted in serious local hyperthermia, which influences not only the cellular nucleus but also cell viability. This occurs either by denaturation of proteins or nucleic acids in the cytoplasm. To show the percentage of apoptotic cells treated with the samples, apoptosis analysis by flow-cytometry was used in the next step.

3.6.2. *Apoptosis analysis by the flow-cytometry method*

Combined chemo-photothermal therapy has been exhibited to be more effective when compared with chemotherapy or photothermal therapy alone since DNA repair procedures are temperature-dependent [13,14]. This higher effect of DNA-damage has been attributed to a stop the replication fork, leading to double-strand breaks creation, which decreases cell viability [14].

Fig. 11 showed the quantitative results of Annexin V-FITC assay. As

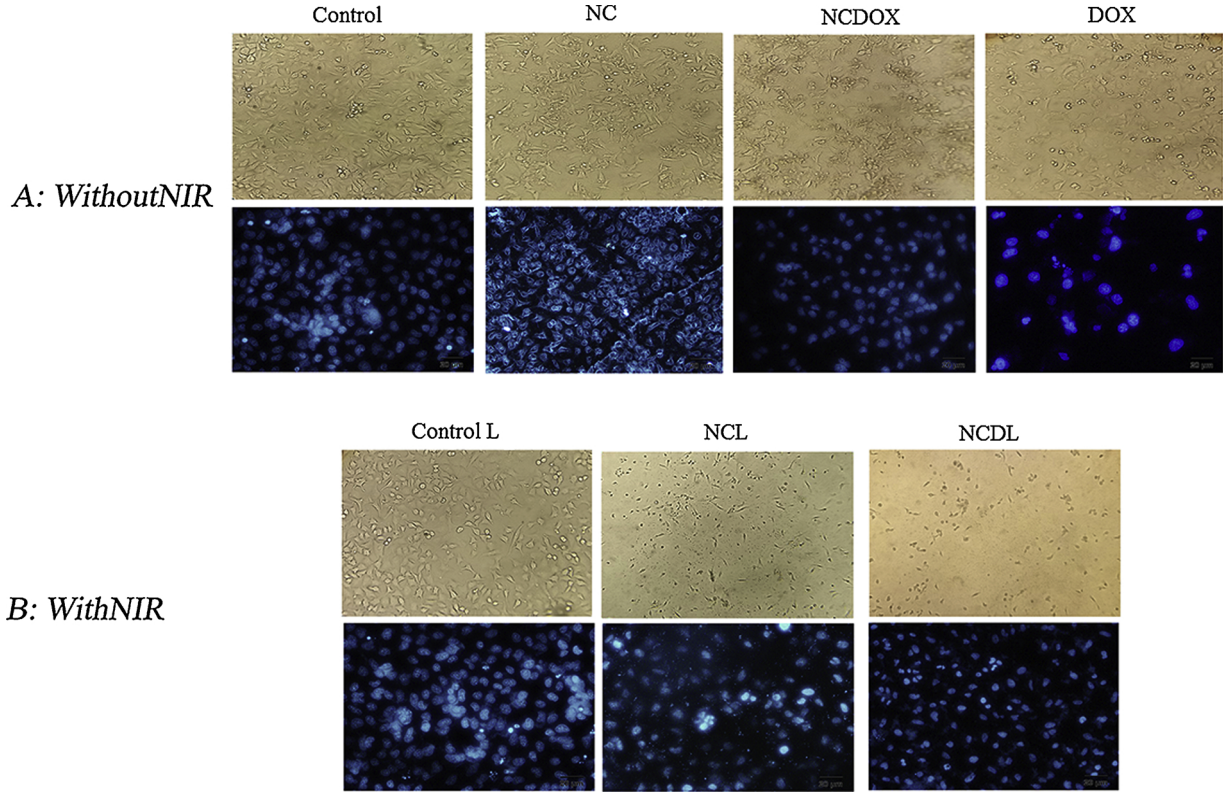

Fig. 10. Fluorescence Microscopic images of DAPI stained MCF7 cells following exposure to SAP@TBP@AuNPs (NC), DOX, DOX-loaded SAP@TBP@AuNPs (NCDOX), laser alone, SAP@TBP@AuNPs (NC) with laser irradiation and DOX-loaded SAP@TBP@AuNPs (NCDOX) with laser irradiation.

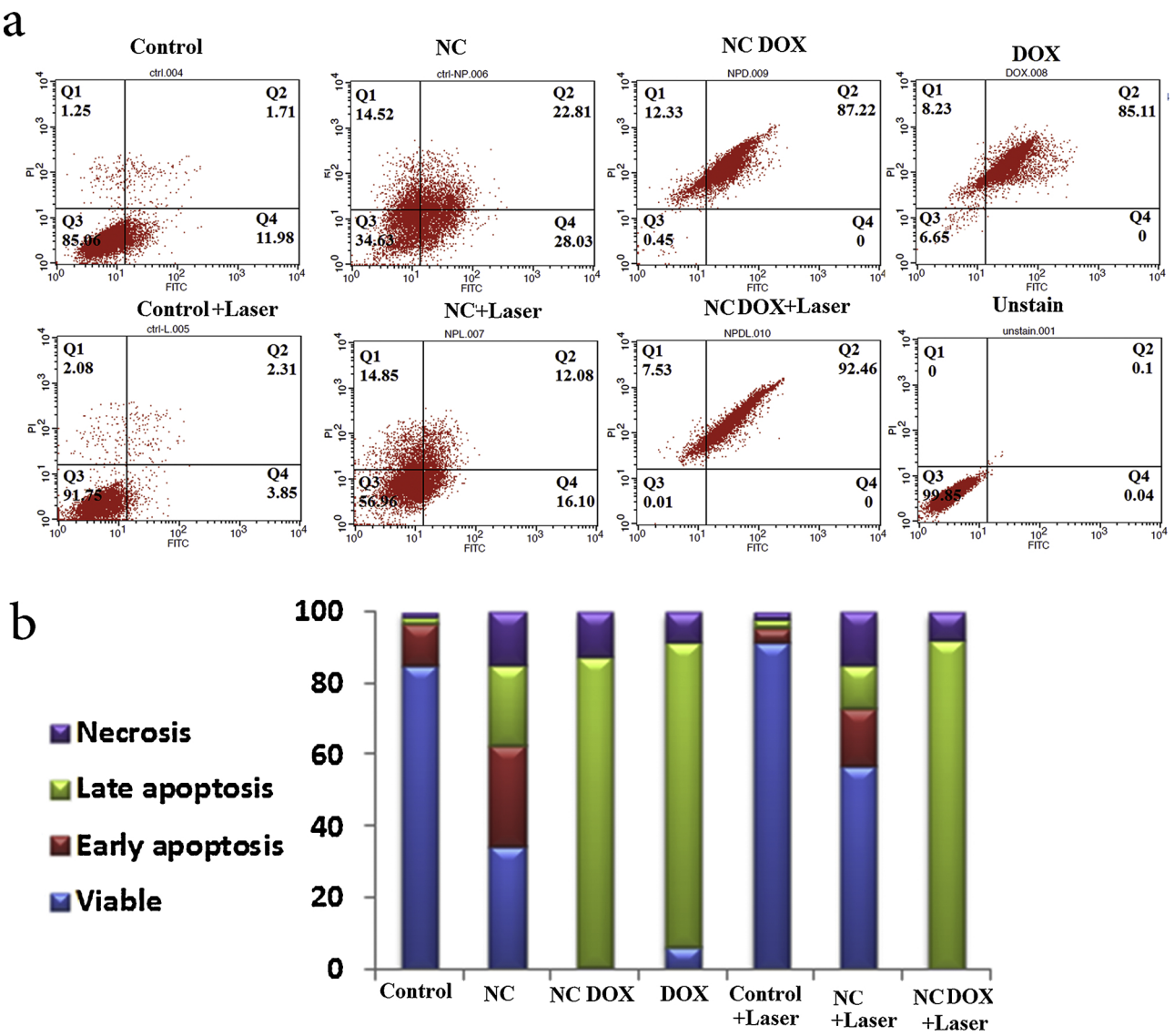

Fig. 11. a) The apoptotic effects of MCF7 cells, determined by flow cytometry, for cells treated with SAP@TBP@AuNPs (NC), DOX, DOX-loaded SAP@TBP@AuNPs (NC DOX), laser alone, SAP@TBP@AuNPs (NC) with laser irradiation and DOX-loaded SAP@TBP@AuNPs (NC DOX) with laser irradiation, b) Quantitative results of apoptotic effects evaluated by Annexin V/FITC assay.

shown in Fig. 11 the cells exposed to DOX-loaded SAP@TBP@AuNPs with laser irradiation showed the maximum population of late apoptosis cells (92.46%) compared to other treatment groups. Also, the cells treated with laser only (810 nm, 0.5 W/cm^2, 10 min) showed more viable cells (viable cells: 91.75%) compared to non-treated control group (viable cells: 85.06%). While in the cells treated with SAP@TBP@AuNPs with laser irradiation the viable cells population fall to 56.96%. Therefore, laser irradiation alone had a proliferative effect and the presence of gold nanoparticles as photo-synthesizer is essential in photothermal therapy. A synergistic effect increase in the combination of chemo-photo therapy in DOX-loaded SAP@TBP@AuNPs with laser irradiation group leading to 99.99% (sum of population of apoptotic and necrotic cells) of viability loss with an increase of 8 °C in temperature (reached to 45 °C).

3.6.3. Cell cycle arrest results

For analyzing DNA content as an index of cell generating, reagents including DNA dye such as propidium iodide (PI) are used. In this study, the cell cycle results showed that the cells treated with only laser irradiation (810 nm, 0.5 W/cm^2, 10 min) or only NPs did not show significant change in the cell cycle pattern of MCF-7 cells compared to untreated cells (Fig. 12). The percentage of sub G0-G1cell population was increased in the cells treated with SAP@TBP@AuNPs with laser irradiation, DOX-loaded SAP@TBP@AuNPs and frees DOX. A large number of the cells were transferred to the G2/M phases and Go/G1 condition after treatment with SAP@TBP@AuNPs with laser irradiation (21.4 and 42.4%) and DOX-loaded SAP@TBP@AuNPs without laser irradiation (35.2 and 33.6%). The treatment group that received both therapy strategies, DOX-loaded SAP@TBP@AuNPs with laser irradiation, was observed notable variation in cell cycle and a shift to sub Go/G1 condition so that highest sub G0-G1 arrest (˜67%) was observed among all treatment groups.

4. Conclusion

In this study, very stable gold hydrosols were synthesized at room temperature and natural pH using amine containing copolymer as reducing and stabilizing agent. Subsequently, gold nanoparticles were decorated with a polymer rich of carboxylic acid groups. The obtained gold nanoparticles had spherical morphology with an average diameter of 30 nm and high DOX loading capacity (100%) and excellent uptake (100%) in MCF-7 breast cancer cells at first exposure hours.

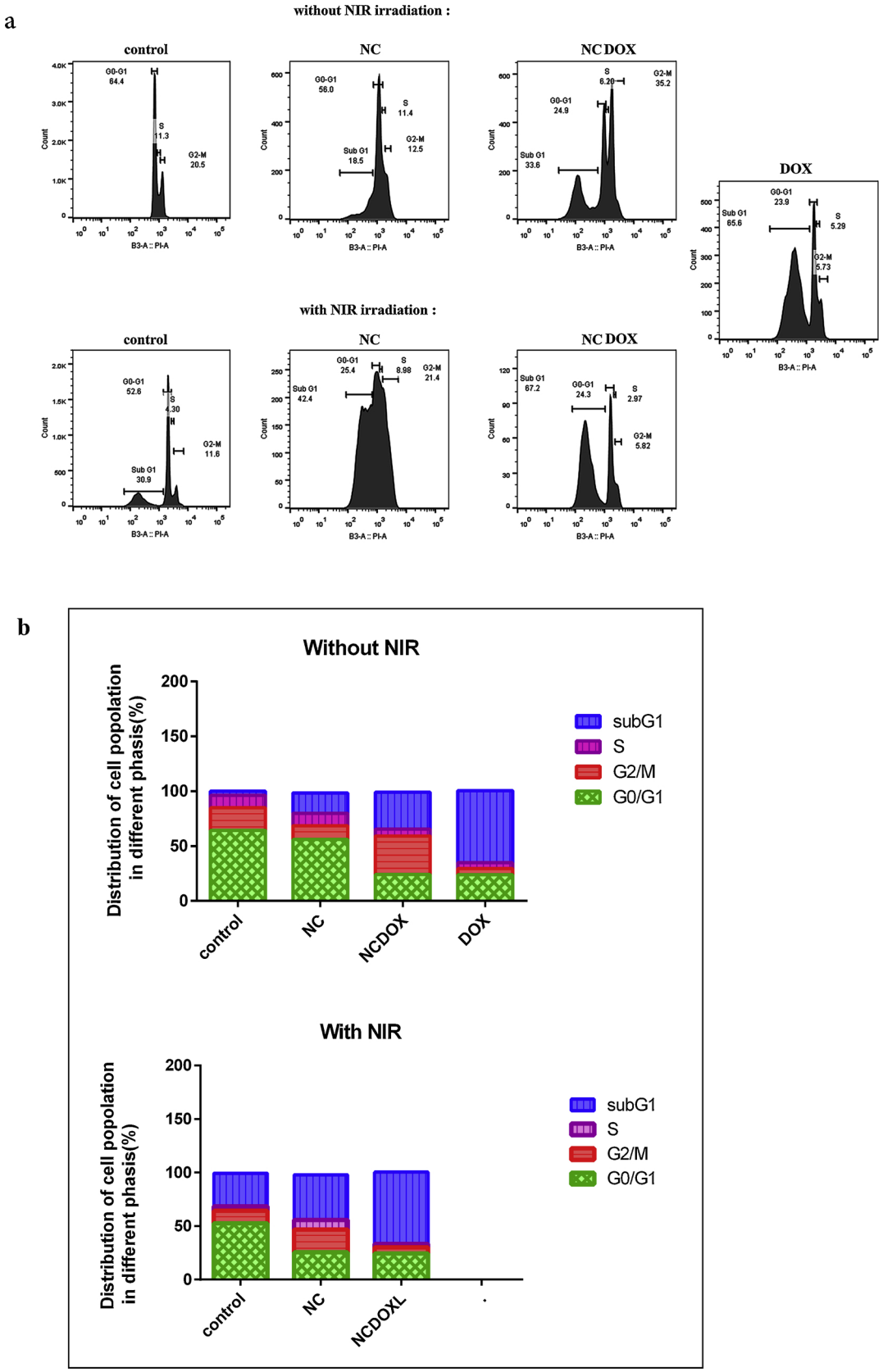

Fig. 12. a) Cell cycle distributions investigated for MCF-7 cells treated with SAP@TBP@AuNPs (NC), DOX, DOX-loaded SAP@TBP@AuNPs (NC DOX), laser alone, SAP@TBP@AuNPs(NC) with laser irradiation and DOX-loaded SAP@TBP@AuNPs (NC DOX) with laser irradiation, b) Quantitative results of cell cycle arrest and distribution.

Nanoparticles irradiated with a NIR laser showed a dramatic increase in temperature up to 45 °C at 10 min, and induced hyperthermia, lead to synergistic effect by enhanced apoptosis cell death. The DAPI staining, cell cycle and Annexin-V assays results indicated that the combination of chemo-photothermal therapy increased the cytotoxicity and apoptosis effect on MCF-7 breast cancer cell lines. The findings of this study could be useful for designing future cancer therapy programs using biochemotherapy combined with photothermal therapy.

Acknowledgments

This study was financially supported by a grant [NO: 95/72] from Drug Applied Research Center, Tabriz University of Medical Sciences, Tabriz, Iran.

References

[1] V. Schirrmacher, From chemotherapy to biological therapy: a review of novel concepts to reduce the side effects of systemic cancer treatment, Int. J. Oncol. 54 (2) (2019) 407–419.
[2] L.R. Hirsch, R.J. Stafford, J.A. Bankson, et al., Nanoshell-mediated near-infrared thermal therapy of tumors under magnetic resonance guidance, Proc. Natl. Acad. Sci. 100 (23) (2003) 13549–13554.
[3] K.F. Chu, D.E. Dupuy, Thermal ablation of tumors: biological mechanisms and advances in therapy [Perspective], Nat. Rev. Cancer 14 (2014) 199 02/24/online.
[4] J. Nam, S. Son, L.J. Ochyl, et al., Chemo-photothermal therapy combination elicits anti-tumor immunity against advanced metastatic cancer, Nat. Commun. 9 (1) (2018) 1074 2018/03/14.
[5] K. König, Multiphoton microscopy in life sciences, J. Microsc. 200 (2) (2000) 83–104.
[6] R. Mendes, P. Pedrosa, J.C. Lima, et al., Photothermal enhancement of chemotherapy in breast cancer by visible irradiation of gold nanoparticles, Sci. Rep. 7 (1) (2017) 10872 2017/09/07.
[7] N.S. Abadeer, C.J. Murphy, Recent progress in cancer thermal therapy using gold nanoparticles, J. Phys. Chem. C 120 (9) (2016) 4691–4716 2016/03/10.
[8] X. Huang, M.A. El-Sayed, Gold nanoparticles: optical properties and implementations in cancer diagnosis and photothermal therapy, J. Adv. Res. 1 (1) (2010) 13–28.
[9] B. Van de Broek, N. Devoogdt, A. D'Hollander, et al., Specific cell targeting with nanobody conjugated branched gold nanoparticles for photothermal therapy, ACS Nano 5 (6) (2011) 4319–4328.
[10] S. Hwang, J. Nam, S. Jung, et al., Gold nanoparticle-mediated photothermal therapy: current status and future perspective, Nanomedicine 9 (13) (2014) 2003–2022.
[11] N. Elbialy, M. Abdelhamid, T. Youssef, Low power argon laser-induced thermal therapy for subcutaneous Ehrlich carcinoma in mice using spherical gold nanoparticles, J. Biomed. Nanotechnol. 6 (6) (2010) 687–693.
[12] X. Wang, G. Li, Y. Ding, et al., Understanding the photothermal effect of gold nanostars and nanorods for biomedical applications, RSC Adv. 4 (57) (2014) 30375–30383.
[13] Q. Tian, M. Tang, Y. Sun, et al., Hydrophilic flower-like CuS superstructures as an efficient 980 nm laser-driven photothermal agent for ablation of cancer cells, Adv. Mater. 23 (31) (2011) 3542–3547.
[14] J. Chen, D. Wang, J. Xi, et al., Immuno gold nanocages with tailored optical properties for targeted photothermal destruction of cancer cells, Nano Lett. 7 (5) (2007) 1318–1322.
[15] S.E. Skrabalak, J. Chen, Y. Sun, et al., Gold nanocages: synthesis, properties, and applications, Acc. Chem. Res. 41 (12) (2008) 1587–1595.
[16] M.P. Melancon, W. Lu, Z. Yang, et al., In vitro and in vivo targeting of hollow gold nanoshells directed at epidermal growth factor receptor for photothermal ablation therapy, Mol. Cancer Ther. 7 (6) (2008) 1730–1739.
[17] N. Li, P. Zhao, D. Astruc, Anisotropic gold nanoparticles: synthesis, properties, applications, and toxicity, Angew. Chem. Int. Ed. 53 (7) (2014) 1756–1789.
[18] H.-Y. Wu, M. Liu, M.H. Huang, Direct synthesis of branched gold nanocrystals and their transformation into spherical nanoparticles, J. Phys. Chem. B 110 (39) (2006) 19291–19294.
[19] C.-H. Kuo, M.H. Huang, Synthesis of branched gold nanocrystals by a seeding growth approach, Langmuir 21 (5) (2005) 2012–2016.
[20] J. Han, J. Li, T. Xu, et al., Coating urchinlike gold nanoparticles with polypyrrole thin shells to produce photothermal agents with high stability and photothermal transduction efficiency, Langmuir 29 (23) (2013) 7102–7110.
[21] J. Hu, C.A. Brackemyer, H. Byun, et al., Enhanced stability of anisotropic gold nanoparticles by poly (N-isopropylacrylamide), J. Mater. Sci. Technol. 30 (5) (2014) 441–448.
[22] B. Van de Broek, F. Frederix, K. Bonroy, et al., Shape-controlled synthesis of NIR absorbing branched gold nanoparticles and morphology stabilization with alkanethiols, Nanotechnology 22 (1) (2010) 015601.
[23] L.-C. Cheng, J.-H. Huang, H.M. Chen, et al., Seedless, silver-induced synthesis of star-shaped gold/silver bimetallic nanoparticles as high efficiency photothermal therapy reagent, J. Mater. Chem. 22 (5) (2012) 2244–2253.
[24] T.S. Hauck, T.L. Jennings, T. Yatsenko, et al., Enhancing the toxicity of cancer chemotherapeutics with gold nanorod hyperthermia, Adv. Mater. 20 (20) (2008) 3832–3838.
[25] H. Park, J. Yang, J. Lee, et al., Multifunctional nanoparticles for combined doxorubicin and photothermal treatments, ACS Nano 3 (10) (2009) 2919–2926 2009/10/27.
[26] J. Nam, W.-G. La, S. Hwang, et al., pH-responsive assembly of gold nanoparticles and "Spatiotemporally concerted" drug release for synergistic cancer therapy, ACS Nano 7 (4) (2013) 3388–3402 2013/04/23.
[27] Z. Zhang, J. Wang, X. Nie, et al., Near infrared laser-induced targeted cancer therapy using thermoresponsive polymer encapsulated gold nanorods, J. Am. Chem. Soc. 136 (20) (2014) 7317–7326 2014/05/21.
[28] H. Chen, Y. Di, D. Chen, et al., Combined chemo- and photo-thermal therapy delivered by multifunctional theranostic gold nanorod-loaded microcapsules [10.1039/C5NR00473J], Nanoscale 7 (19) (2015) 8884–8897.
[29] S. Wang, S. Wang, X. Zhao, et al., Biologically inspired polydopamine capped gold nanorods for drug delivery and light-mediated cancer therapy, ACS Appl. Mater. Interfaces 8 (37) (2016) 24368–24384 2016/09/21.
[30] P. Wust, B. Hildebrandt, G. Sreenivasa, et al., Hyperthermia in combined treatment of cancer, Lancet Oncol. 3 (8) (2002) 487–497.
[31] L. Schaaf, M. Schwab, C. Ulmer, et al., Hyperthermia synergizes with chemotherapy by inhibiting PARP1-dependent DNA replication arrest, Cancer Res. (2016) canres. 2908.2015.
[32] O. Tacar, P. Sriamornsak, C.R. Dass, Doxorubicin: an update on anticancer molecular action, toxicity and novel drug delivery systems, J. Pharm. Pharmacol. 65 (2) (2013) 157–170.
[33] V. Mourya, N.N. Inamdar, A. Tiwari, Carboxymethyl chitosan and its applications, Adv. Mater. Lett. 1 (1) (2010) 11–33.
[34] H. Huang, Q. Yuan, X. Yang, Preparation and characterization of metal–chitosan nanocomposites, Colloids Surf. B Biointerfaces 39 (1–2) (2004) 31–37.
[35] A. Gharatape, R. Salehi, Recent progress in theranostic applications of hybrid gold nanoparticles, Eur. J. Med. Chem. 138 (2017) 221–233.
[36] C. Feng, L. Gu, D. Yang, et al., Size-controllable gold nanoparticles stabilized by PDEAEMA-based double hydrophilic graft copolymer, Polymer 50 (16) (2009) 3990–3996.
[37] G. Mountrichas, S. Pispas, E.I. Kamitsos, Effect of temperature on the direct synthesis of gold nanoparticles mediated by poly (dimethylaminoethyl methacrylate) homopolymer, J. Phys. Chem. C 118 (39) (2014) 22754–22759.
[38] E. Baygazieva, N. Yesmurzayeva, G. Tatykhanova, et al., Polymer protected gold nanoparticles: synthesis, characterization and application in catalysis, Int. J. Biol. Chem. 7 (1) (2014) 14–23.
[39] E.B.N.Y.G. Tatykhanova, Kudaibergenov GMVKS, Polymer Protected Gold Nanoparticles: Synthesis, Characterization and Application in Catalysis, (2015).
[40] J. Du, J. Bai, Y. Li, et al., One-pot synthesis of polyacrylamide-gold nanocomposite, Mater. Chem. Phys. 106 (2–3) (2007) 412–415.
[41] D. Kessel, Reversible effects of photodamage directed toward mitochondria, Photochem. Photobiol. 90 (5) (2014) 1211–1213.
[42] R.R. Letfullin, C.B. Iversen, T.F. George, Modeling nanophotothermal therapy: kinetics of thermal ablation of healthy and cancerous cell organelles and gold nanoparticles, Nanomed. Nanotechnol. Biol. Med. 7 (2) (2011) 137–145.
[43] S. Bhattacharjee, D. Ershov, J. Gucht, et al., Surface charge-specific cytotoxicity and cellular uptake of tri-block copolymer nanoparticles, Nanotoxicology 7 (1) (2013) 71–84.
[44] X. Li, Y. Tang, L. Xu, et al., Dependence between cytotoxicity and dynamic subcellular localization of up-conversion nanoparticles with different surface charges, RSC Adv. 7 (53) (2017) 33502–33509.
[45] E. Fröhlich, The role of surface charge in cellular uptake and cytotoxicity of medical nanoparticles, Int. J. Nanomedicine 7 (2012) 5577.
[46] X.R. Shao, X.Q. Wei, X. Song, et al., Independent effect of polymeric nanoparticle zeta potential/surface charge, on their cytotoxicity and affinity to cells, Cell Prolif. 48 (4) (2015) 465–474.
[47] S. Honary, F. Zahir, Effect of zeta potential on the properties of nano-drug delivery systems-a review (Part 2), Trop. J. Pharm. Res. 12 (2) (2013) 265–273.
[48] S. Honary, F. Zahir, Effect of zeta potential on the properties of nano-drug delivery systems-a review (Part 1), Trop. J. Pharm. Res. 12 (2) (2013) 255–264.
[49] A. Gharatape, M. Milani, S.H. Rasta, et al., A novel strategy for low level laser-induced plasmonic photothermal therapy: the efficient bactericidal effect of biocompatible AuNPs@(PNIPAAM-co-PDMAEMA, PLGA and chitosan), RSC Adv. 6 (112) (2016) 110499–110510.
[50] J.R. Seo, H.W. Choi, E.-J. Kim, et al., Facile synthesis of surfactant-free Au decorated hollow silica nanoparticles for photothermal applications, Macromol. Res. 26 (12) (2018) 1129–1134.
[51] X. Liu, Y. Chen, H. Li, et al., Enhanced retention and cellular uptake of nanoparticles in tumors by controlling their aggregation behavior, ACS Nano 7 (7) (2013) 6244–6257.
[52] J. Nam, N. Won, H. Jin, et al., pH-induced aggregation of gold nanoparticles for photothermal cancer therapy, J. Am. Chem. Soc. 131 (38) (2009) 13639–13645 2009/09/30.
[53] S. Hwang, S. Jung, J. Nam, et al., Theragnostic pH-sensitive gold nanoparticles for the selective surface enhanced Raman scattering and photothermal cancer therapy, Anal. Chem. 85 (16) (2013) 7674–7681 2013/08/20.

[54] R.M. CABRAL, P.V. Baptista, The chemistry and biology of gold nanoparticle-mediated photothermal therapy: promises and challenges, Nano Life 3 (3) (2013) 1330001.
[55] H. Jang, Y.-K. Kim, H. Huh, et al., Facile synthesis and intraparticle self-catalytic oxidation of dextran-coated hollow Au–Ag nanoshell and its application for chemo-thermotherapy, ACS Nano 8 (1) (2014) 467–475.
[56] L. Au, D. Zheng, F. Zhou, et al., A quantitative study on the photothermal effect of immuno gold nanocages targeted to breast cancer cells, ACS Nano 2 (8) (2008) 1645–1652.
[57] R. Zhang, S. Su, K. Hu, et al., Smart micelle@ polydopamine core–shell nanoparticles for highly effective chemo–photothermal combination therapy, Nanoscale 7 (46) (2015) 19722–19731.
[58] Y. Zhang, X. Zhan, J. Xiong, et al., Temperature-dependent cell death patterns induced by functionalized gold nanoparticle photothermal therapy in melanoma cells, Sci. Rep. 8 (1) (2018) 8720.